Supporting Information

Tuning Interlayer Stacking of Vinylene-linked Covalent Organic Framework for Enhanced Sacrificial Agent-Free Hydrogen Peroxide Photoproduction

Qiujian Xie[§], Anqi Chen[§], Xiaofeng Li, Chen Xu, Shuai Bi, Weijie Zhang, Juntao Tang, Chunyue Pan, Fan Zhang[*] and Guipeng Yu[*]

Table of Contents

1. Materials

The precursors such as ethyl acitimidate hydrochloride (95%) and 4-Formylbenzeneboronic acid (98%) and 1,3,5-tribromobenzene (98%) were purchased from Energy Chemical Inc. and used as received without further purification. 2,4,6-trimethyl-1,3,5-triazine (TMT) [1] and 1,3,5-tris(4-formylphenyl)benzene (TFPB) [2] was synthesized following literature procedure. All the solvents used for the synthesis were commercially available and used without further purification.

2. General methods

Nitrogen sorption isotherms were performed on an Autosorb iQ (Quantachrome) instrument at 77K using a Brunauer-Emmett-Teller (BET) model ranger from 0.01 to 0.1 bar. All samples were degassed at 150 ℃ for 24 hours before the gas adsorption experiment. And pore size distributions were calculated using the non-local density functional theory (NLDFT) method in the Quadrawin software. Fourier transform infrared spectroscopy (FTIR) analyses of samples were carried on Varian 640IR spectrometer equipped with an ATR cell in the 600-4000 cm^{-1} region. Solution ^{1}H nuclear magnetic resonance (NMR) for the samples dissolved in suitable solvents were obtained on Bruker Avance II 200 spectrometer with tetramethylsilane as the internal reference. Solid-state ^{13}C NMR experiments were performed on a Bruker AVANCE III 400 spectrometer operating at 100.6 MHz. A double resonance 4 mm MAS NMR probe was used at a spinning rate of 5 kHz.

Powder X-ray diffraction (PXRD) data was collected on a RINT-2000 instrument (Rigaku Corporation) using a CuKα anode (λ = 0.154178 Å) radiation operating at 20 kV and 20 mA. Samples were ground and mounted as loose powders onto a silica glass sample holder. All the samples were recorded in the 2θ range of 3-30 degrees with a step size of 0.02 degrees and an exposure time of 0.06 seconds per step. PXRD simulation were performed using the Reflex module in the Materials Studio 6.0. SEM measurements were performed on a FEI Sirion-200 field emission scanning electron microscope. Solid state diffuse reflectance UV-Vis-NIR measurements were obtained using a Agilent Cary-5000 spectrometer.

Photoluminescence (PL) emission spectra and PL decay spectra were measured at room temperature on a FLS1000 spectrophotometer (Edinburgh Instruments, UK). Slits were set to 4 nm for excitation and 2 nm for emission, while the integration time was 0.5 s and the increment 1 nm. The sample was excited at 365 nm, and emission spectra were recorded in a suitable range centred around the emission maximum between 370 and 700 nm. The solid samples of CTFs (5 mg) were mixed with 10 wt% PTFE and 2 mL ethanol under ultrasonication for 30 min to obtain a well-dispersed suspension. 50 μL of the suspension was dropped onto a piece of fluoride-tin oxide (FTO) glass substrates with a cover area of 0.25 cm^2 and the uncovered parts of the electrode were coated with epoxy. Then the working electrode was obtained after drying in air naturally. The photocurrents were recorded by an electrochemical workstation (CHI650E) equipped with a conventional three-electrode cell. A platinum plate electrode and an Ag/AgCl electrode were used as the counter electrode and the reference electrode, respectively. The electrodes were immersed in a 0.2 M Na_2SO_4 aqueous solution for 30 s before measurement. The working electrode was illuminated by

a 300 W Xe lamp (PLS-SXE300C) with a 420 nm cut-off filter from the backside to minimize the impact of thickness of the semiconductor layer. Each measurement was repeated three times under ambient conditions. The electrochemical impedance measurements were performed in dark at open-circuit voltage with AC amplitude of 5 mV in the frequencies range of 0.01 Hz to 10^5 Hz. The electron spin resonance (ESR) signals of the radicals that spin-trapped by 2,2,6,6-tetramethylpiperidine-1-oxyl (TEMPO) or 5,5-dimethyl-1-pyrroline N-oxide (DMPO) were recorded on the JES FA200 spectrometer (JEOL, Japan).

3. Synthetic procedures

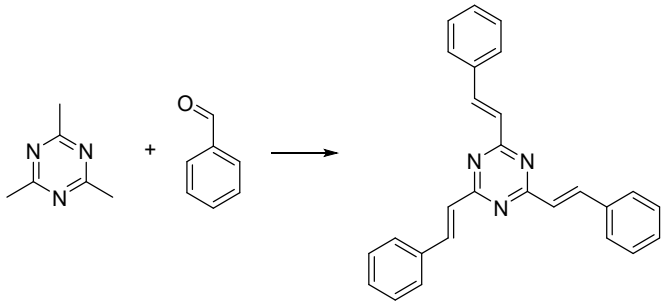

Synthesis of 2,4,6 tristyryl s-triazine (TST, model compound): A 100 mL round bottom flask was charged with 2,4,6-Trimethyl-1,3,5-triazine (TMT) (123 mg, 1.0 mmol), benzaldehyde (381.6 mg, 3.6 mmol), KOH (3.16 g, 20 wt%) and 20 mL CH_3OH then heated up to 50 ℃ for 24 hours under nitrogen atmosphere. After removal of solvent, the pure model compound as white solid was obtained from the recrystallization in the mixed solution of dichloromethane/ethanol. Yield: 90% (346.6mg).

^{1}H NMR (400 MHz, $CDCl_3$) δ 8.23 (d, J = 16.0 Hz, 1H), 7.63 (d, J = 4 Hz, 2H), 7.388-7.32 (m, 3H), 7.12 (d, J = 16.0 Hz, 1H); ^{13}C NMR (100 MHz, $CDCl_3$) δ 170.28, 140.65, 134.50, 128.46, 127.78, 127.13, 125.29.

General synthesis procedure for sp^{2}c-CTF-4@AA: 2,4,6-Trimethyl-1,3,5-triazine (TMT) (61.58 mg, 0.5 mmol), 1,3,5-tris(4-formylphenyl) benzene (TFPB) (195.22 mg, 0.5 mmol) and sodium ethoxide (102.08 mg, 1.5 mmol) were dissolved in a binaryl solvent of 7 mL n-butanol and 3 mL 1,2-dichlorobenzene. This mixture was heated up to 120 ℃ for a 3-day reaction. The resulting precipitates were collected and washed with methanol, tetrahydrofuran, acetone, and dichloromethane in sequence for three times (10 mL for each), and then dried under vacuum at 120 °C for 12 h. The target sp^{2}c-CTF-4@AA was achieved as pale-yellow powder (yield: 87%).

General synthesis procedure for sp^{2}c-CTF-4@AB: A similar protocol to the synthesis of sp2c-CTF-4@AA was used while a base catalyst, i.e. Lithium hydroxide was used. 2,4,6-Trimethyl-1,3,5-triazine (TMT) (12.3 mg, 0.1 mmol), 1,3,5-tris(4-formylphenyl)-benzene (TFPB) (39.1 mg, 0.1 mmol) were dissolved in a binaryl solvent of 1.5 mL 1,2-dichlorobenzene and 0.5 mL N, N-dimethylformamide, then added 0.1 mL 1 M LiOH/CH_3OH. This mixture was heated up to 120 ℃ for a 3-day reaction. The solid was filtered, washed with water, ethanol and THF, then allowed to further drying step under vacuum at 100 °C. Finally, pure sp^{2}c-CTF-4@AB sample was afforded as yellow (fluffy) powder (yield: 86%).

Photocatalytic H_2O_2 production: 5 mg of polymers (sp^{2}c-CTF-4@AA and sp^{2}c-CTF-4@AB)

were weighed into 15 mL photocatalytic vials, and 10 mL of ultrapure water was added, and ultrasonication was performed for 30 min to make the polymers well dispersed in the water, and then oxygen was passed into the vials for 30 min to saturate the system with oxygen in the dark, which was continued to be passed into the vials when the catalytic reaction was catalyzed. Afterwards, the reaction bottle was put into the 40 W blue LED light source for illumination, and circulating cooling water was passed in and stirring was turned on. When the reaction reached equilibrium, the photocatalytic reaction was terminated, and the reaction solution (0.2 mL) was taken and filtered through microporous membrane to remove the catalyst, and then stored in a light-proof place as the sample to be tested.

H_2O_2 detection methods: DPD colorimetric was used for the detection of H_2O_2 concentration. The generated H_2O_2 was added dropwise in PBS buffer to keep the solution neutral and prevent the decomposition of H_2O_2 due to heat as well as pH environment. In the presence of POD, H_2O_2 decomposes to produce ·OH, which subsequently reacts with DPD, converting the colorless DPD to pink DPD^+, which in turn develops the color. The yield of H_2O_2 was obtained by performing a liquid UV test of this process.

4. Results and Discussion

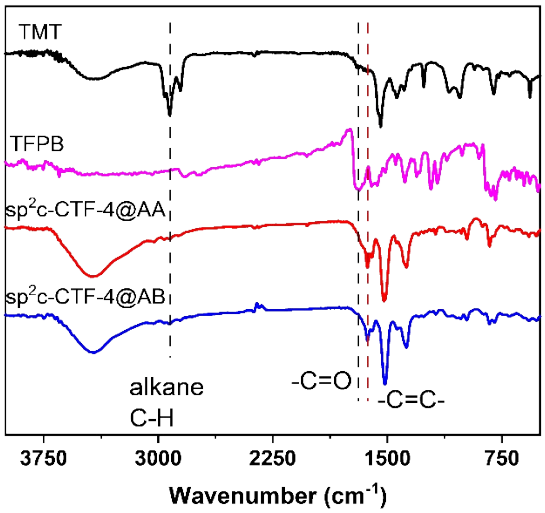

Figure S1. Comparison FTIR spectra of sp^2c-CTF-4, 2,4,6-Trimethyl-1,3,5-triazine (TMT) and 1,3,5-tris(4-formylphenyl) benzene (TFPB).

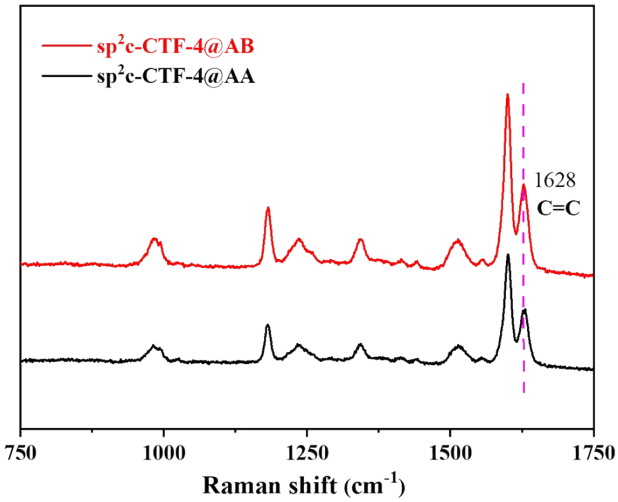

Figure S2. Raman spectra of sp²c-CTF-4@AA and sp²c-CTF-4@AB.

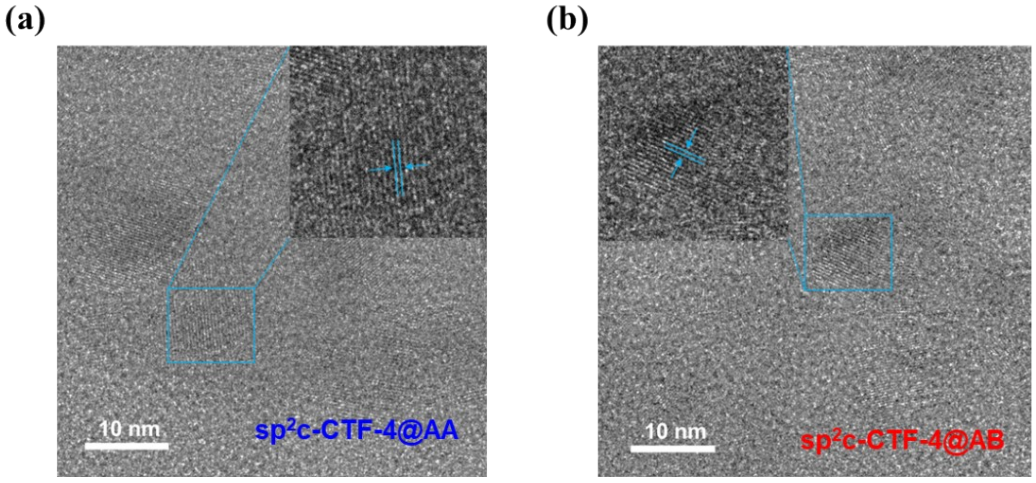

Figure S3. HRTEM images of sp^2c-CTF-4@AA and sp^2c-CTF-4@AB.

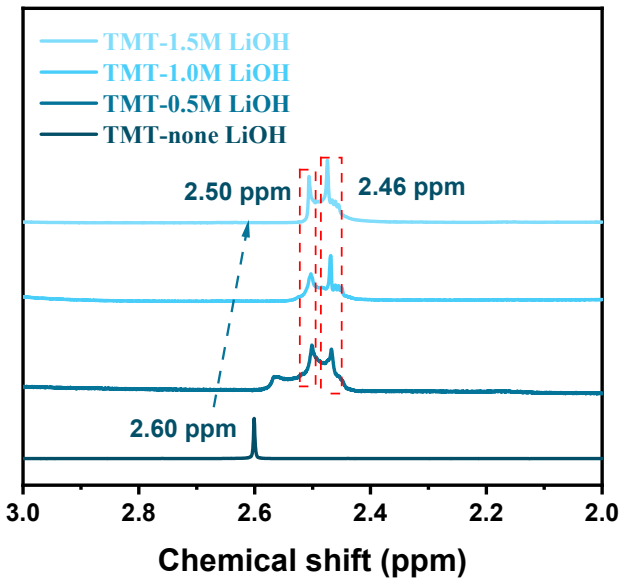

Figure S4. In situ ^{1}H-NMR spectroscopic measurements of sp^{2}c-CTF-4@AB.

First-principles computations based on density functional theory (DFT) were implemented in the Vienna Ab initio simulation package (VASP)[3]. The generalized gradient approximation (GGA) involving Perdew, Burke, and Ernzerhof (PBE)[4] was used for calculating the exchange-correlation energy. A 400 eV cutoff energy was adopted for the plane-wave basis set in conjunction with the projector augmented wave (PAW)[5]. The energy and force convergence were set to be 1E-4 eV and 0.02 eV $Å^{-1}$, respectively. The Brillouin zone was sampled using a Γ-centered 2*2*4 k-point mesh. In all the computations, a DFT-D3 method was added to describe the van der Waals interactions[6]. The calculation of the X-ray diffraction (XRD) patterns was carried out by using the Powder Diffraction function in Reflex module included in software Materials Studio[7].

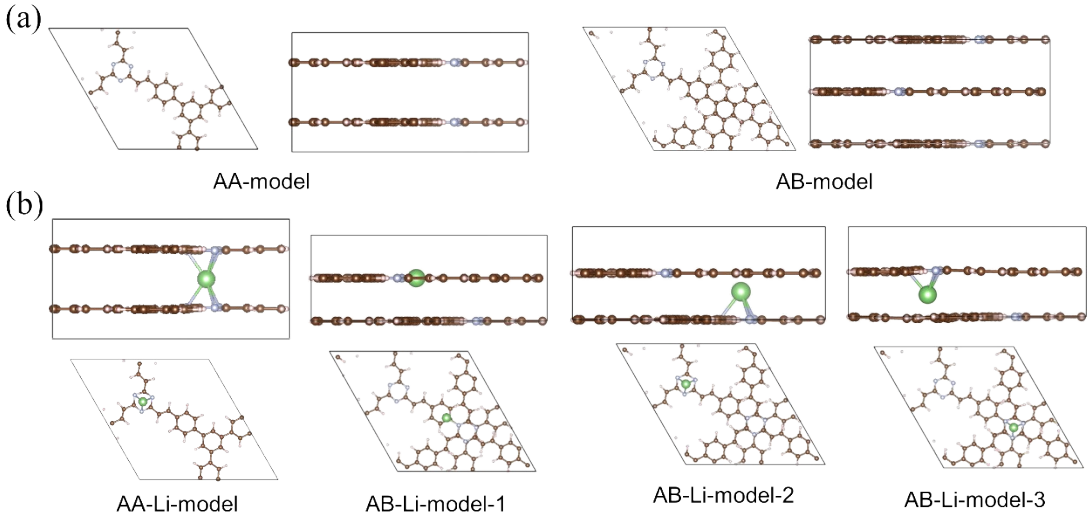

Figure S5. DFT-D3-optimized structures of the AA and AB stacking model (a) without or (b) with Li^+ of sp^2c-CTF-4.

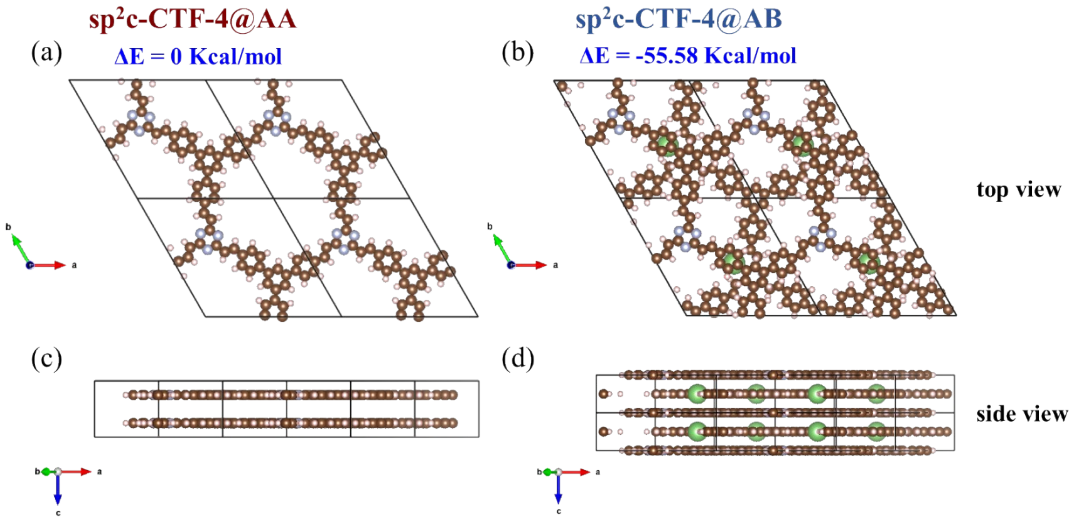

Figure S6. DFT-D3-optimized structures of the AA and AB stacking orders, together with their energy difference (based on the unit cell) of (a) sp^2c-CTF-4@AA without Li^+ and (b) sp^2c-CTF-4@AB with Li^+.

Table S1. Summary of the total energy of the structures of the AA and AB stacking model.

E(eV)	AA	AA-Li-model	AB
	-800.26	-798.27	-800.30
	AB-Li-model-1	AB-Li-model-2	AB-Li-model-3
	-802.41	-801.56	-802.03

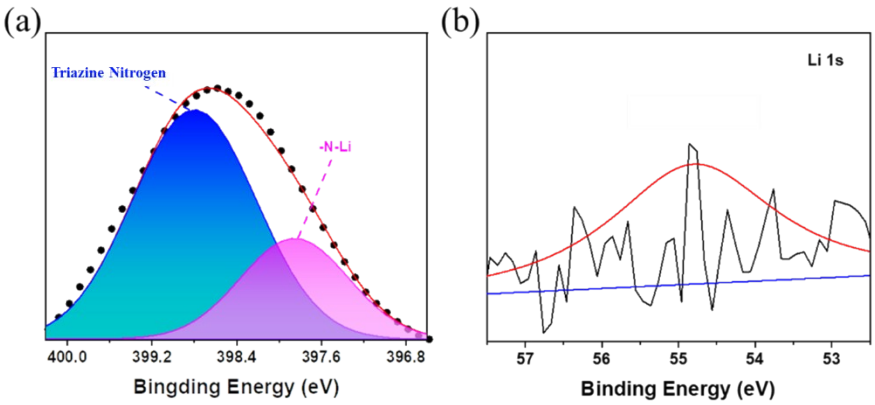

Figure S7. XPS spectra of (a) N 1s and (b) Li 1s for sp^2c-CTF-4@AB after treated in aqueous saturated KOH methanol/water=1/1 solution 72 hours and ultrasonic for 12 hours.

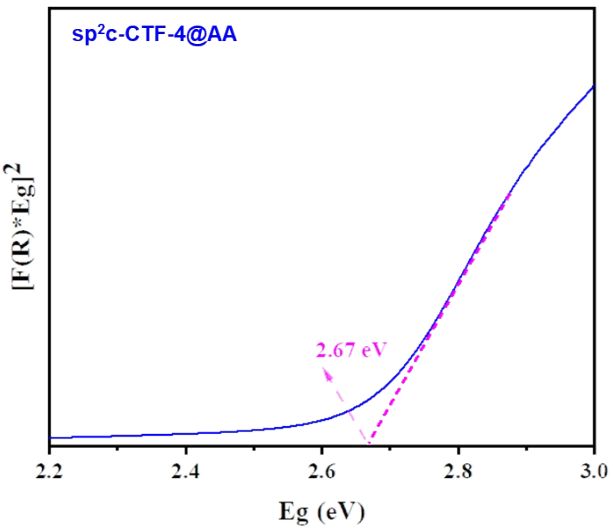

Figure S8. Tauc plots of the transformed Kubelka-Munk function *vs*. the energy of sp²c-CTF-4@AA.

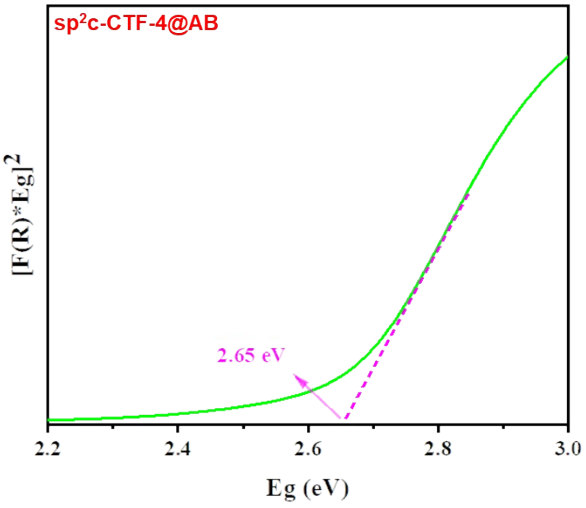

Figure S9. Tauc plots of the transformed Kubelka-Munk function *vs*. the energy of sp²c-CTF-4@AB.

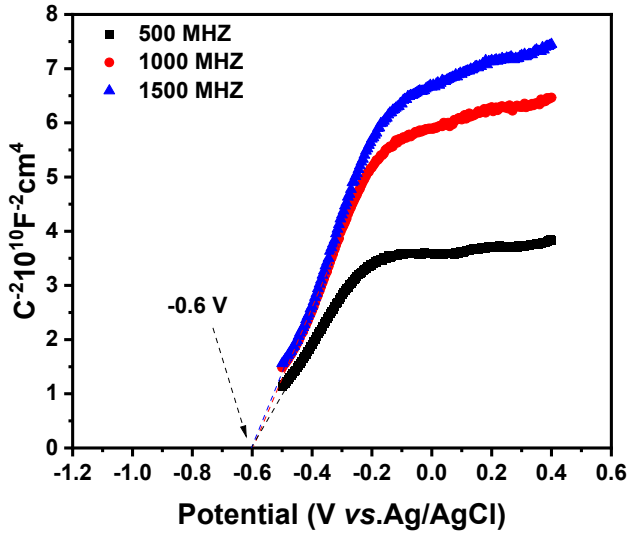

Figure S10. Mott−Schottky plot of sp^{2}c-CTF-4@AA.

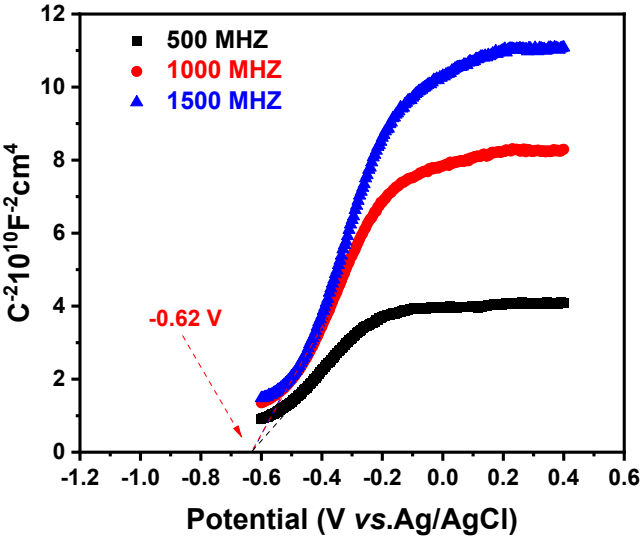

Figure S11. Mott−Schottky plot of sp^{2}c-CTF-4@AB.

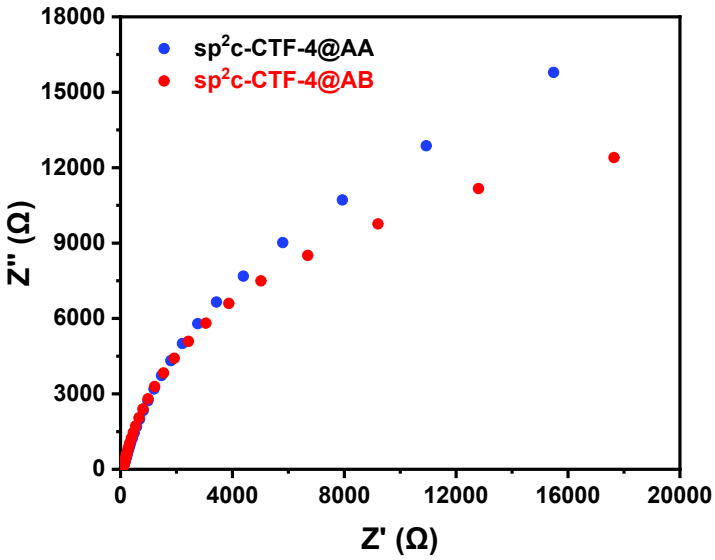

Figure S12. Electrochemical impedance spectroscopy of sp²c-CTF-4@AA and sp²c-CTF-4@AB.

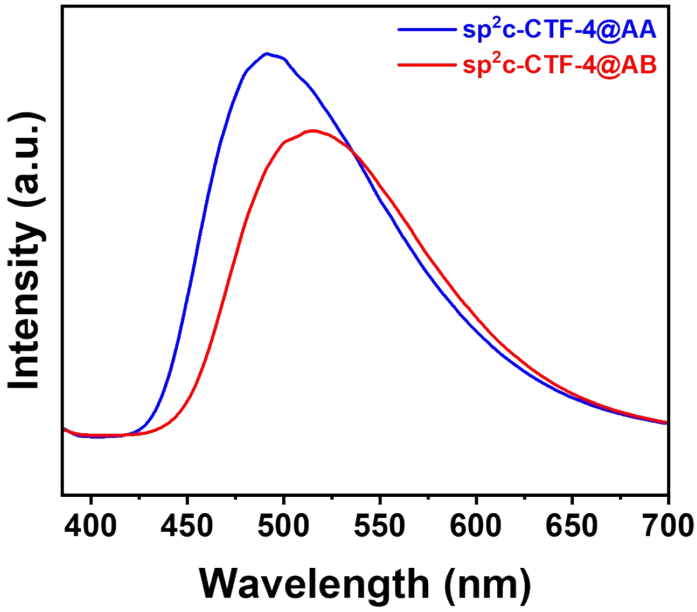

Figure S13. Photoluminescence (PL) emission spectra of sp^2c-CTF-4@AA and sp^2c-CTF-4@AB in the solid-state.

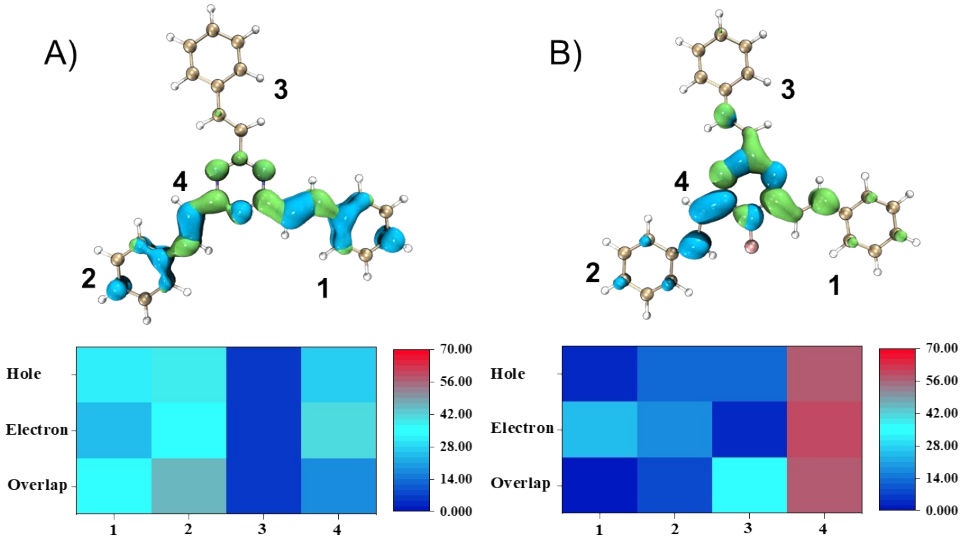

Figure S14. Electrons-holes distribution (Green represent electron; Blue represent Hole) and transition density matrix heat map of electrons-holes contribution distribution for excited-fragments of (A) sp^2c-CTF-4@AA, (B) sp^2c-CTF-4@AB.

Table S2. Summary of photocatalytic H_2O_2 evolution rates of most reported COF-based photocatalysts.

Photocatalysts	Reaction Condition	Solvent	H_2O_2 (μmol/h/g)	Ref
CTF-BDDBN	λ>420 nm	H_2O	97.2	[8]
TAPD-$(Me)_2$COF	λ=420~700 nm	H_2O : EtOH=9:1	97	[9]
SonoCOF-F2	λ>420 nm	H_2O	164	[10]
TAPQ-COF-12	λ>420 nm	H_2O	420	[11]
TiCOF-spn	\	\	489.94	[12]
COF-TfpBpy	λ > 420 nm	H_2O	695	[13]
TDB-COF	λ>420 nm	H_2O	723.5	[14]
COF-nust-8	λ>420 nm	H_2O : EtOH=9:1	1081	[15]
COF-TAPB-BPDA	λ>420 nm	H_2O : BA=4:1	1240	[16]
Py-Da-COF	λ>420 nm	H_2O : BA=9:1	1242	[17]
TPB-DMTP-COF	λ>420 nm	H_2O	1565	[18]
DETH-COF	λ=450 nm	H_2O	1665	[19]
TF_{50}-COF	λ>400 nm	H_2O : EtOH=9:1	1739	[20]
HEP-TAPT-COF	λ > 420 nm	H_2O	1750	[21]
EBA-COF	λ=420 nm	H_2O : EtOH=9:1	1830	[22]
CoPc-BTM-COF	λ>400 nm	H_2O : EtOH=9:1	2096	[23]
TAPB-PDA-OH	λ=420 nm	H_2O : EtOH=9:1	2117.6	[24]
COF-TTA-TTTA	λ = 420 nm	H_2O	2406	[25]
DMCR-1NH	λ=420-700 nm	Water : IPA=10:1	2588	[26]
CN-COF	λ>400 nm	H_2O : EtOH=9:1	2623	[27]
sp^2c-CTF-4@AA sp^2c-CTF-4@AB	λ>420 nm	H_2O H_2O	1020 2758	This work

TPB-DMTP-COF	λ>420 nm	H_2O	2882	[28]
Bpt-CTF	350-780 nm	H_2O	3268.1	[29]
FS-COFs	λ>420 nm	H_2O	3904	[30]
Bpy-TAPT	λ>420 nm	H_2O	4038	[31]
TAH-COF	λ>420 nm	H_2O	6003	[32]

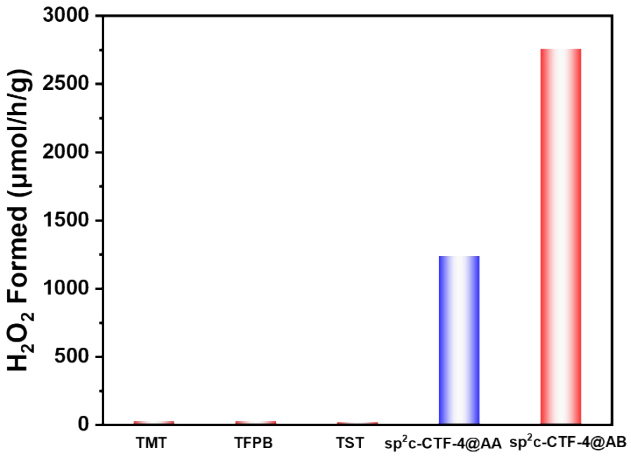

Figure S15: Comparison of photocatalytic H_2O_2 production performance of monomer (TMT, TFPB), model product (TST) and sp^{2}c-CTF-4;

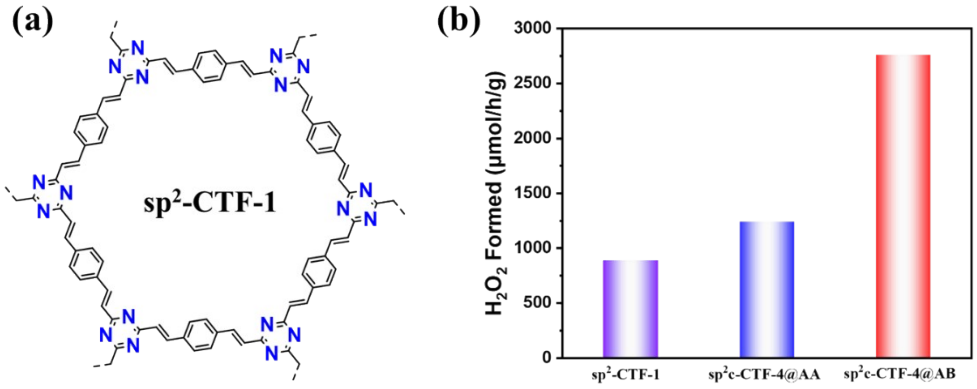

Figure S16: Comparison of photocatalytic H_2O_2 production performance of sp^2-CTF-1and sp^{2}c-CTF-4;

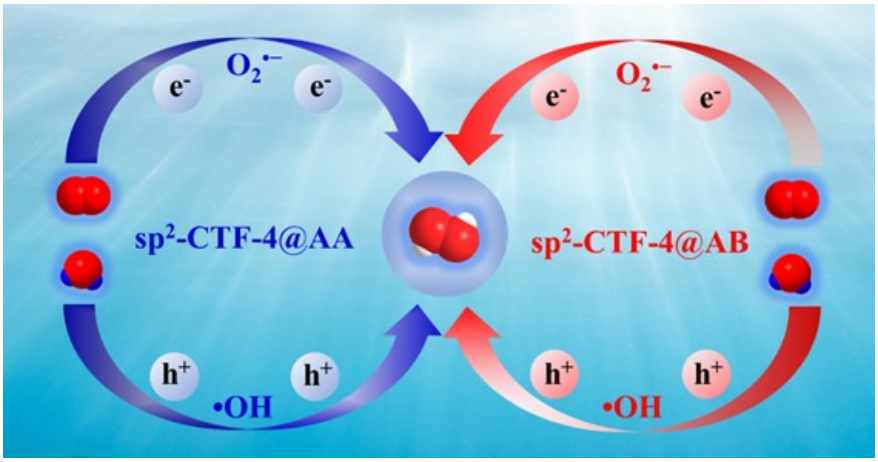

Figure S17: Mechanism of photocatalytic H_2O_2 production.

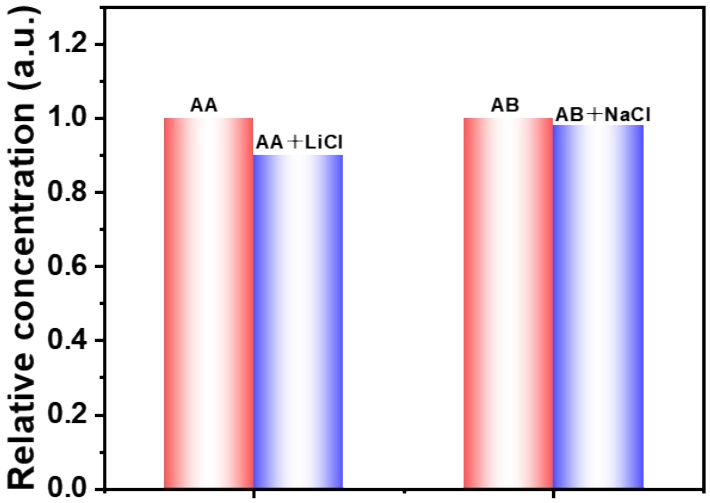

Figure S18. Differences in H_2O_2 production performance of sp^2c-CTF-4@AA and sp^2c-CTF-4@AB by addition of alkali catalysts (Li^+:0.03%; Na^+:0.01%).

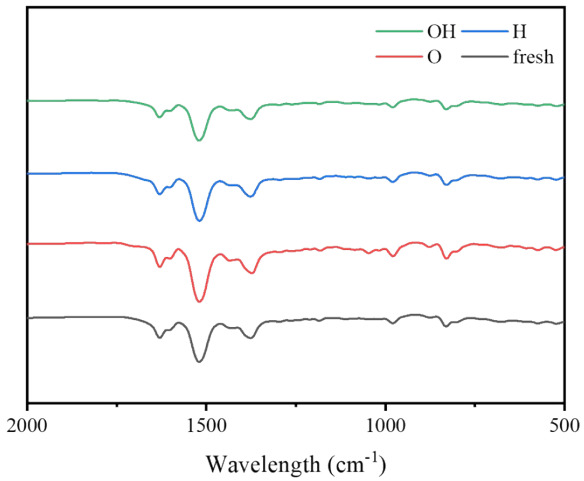

Figure S19. FTIR spectra of pristine sp^{2}c-CTF-4@AA (black), 72 hours treated in aqueous 35% H_2O_2 for 72 hours (red), concentrated 12M HCl (blue), and saturated KOH methanol/water=1/1 solution (green).

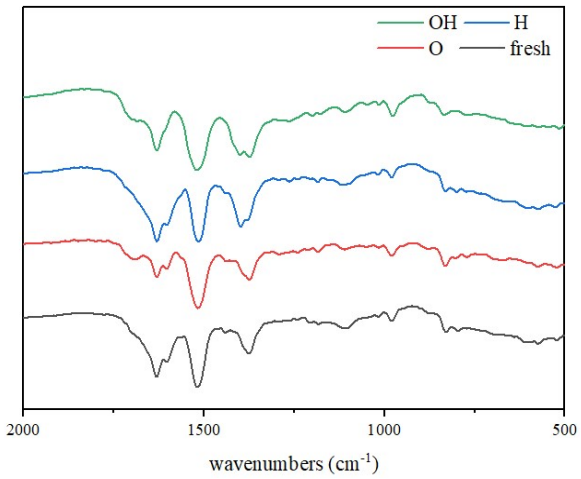

Figure S20. FTIR spectra of pristine sp^{2}c-CTF-4@AB (black), 72 hours treated in aqueous 35% H_2O_2 for 72 hours (red), concentrated 12M HCl (blue), and saturated KOH methanol/water=1/1 solution (green).

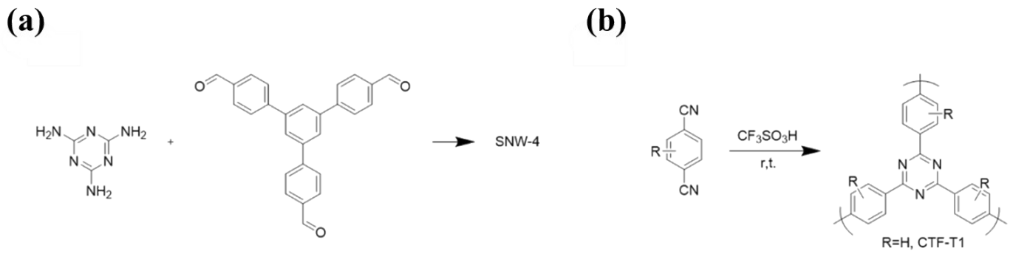

Figure S21. Schematic structure of SNW-4[33] and CTF-T1[34].

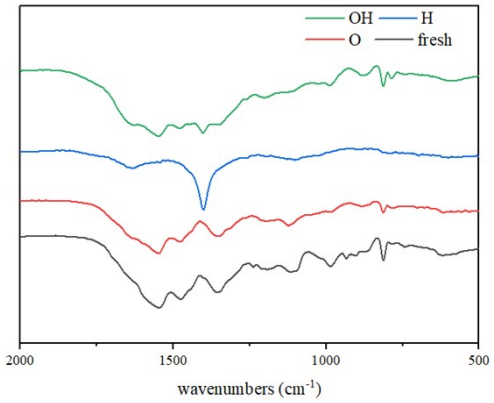

Figure S22. FTIR spectra of pristine SNW-4 (black), 72 hours treated in aqueous 35% H_2O_2 for 72 hours (red), concentrated 12M HCl (blue), and saturated KOH methanol/water=1/1 solution (green).

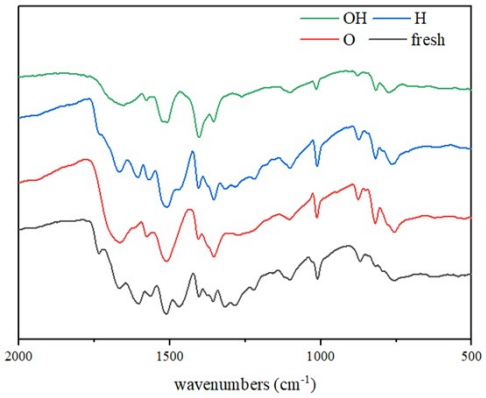

Figure S23. FTIR spectra of pristine CTF-T1 (black), 72 hours treated in aqueous 35% H_2O_2 for 72 hours (red), concentrated 12M HCl (blue), and saturated KOH methanol/water=1/1 solution (green).

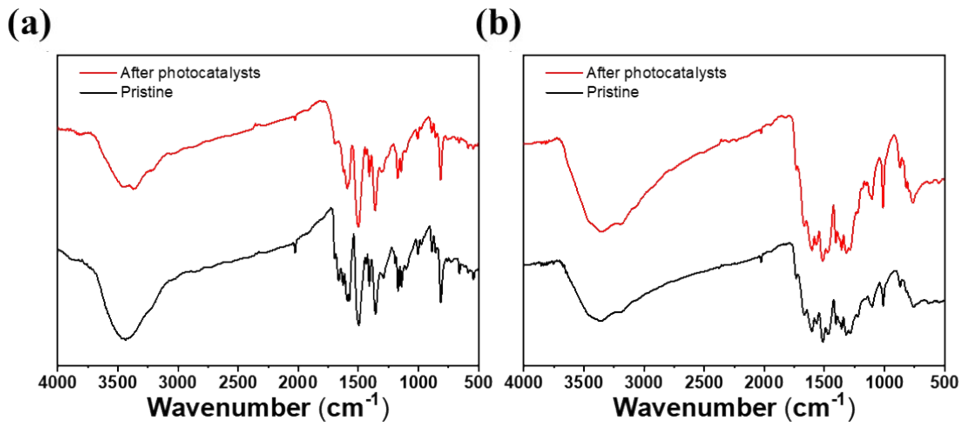

Figure S24. (a) FTIR spectra of pristine SNW-4 (black) and after photocatalysts (red); **(**b) FTIR spectra of pristine CTF-T1 (black) and after photocatalysts (red).

5. NMR Spectra of monomers

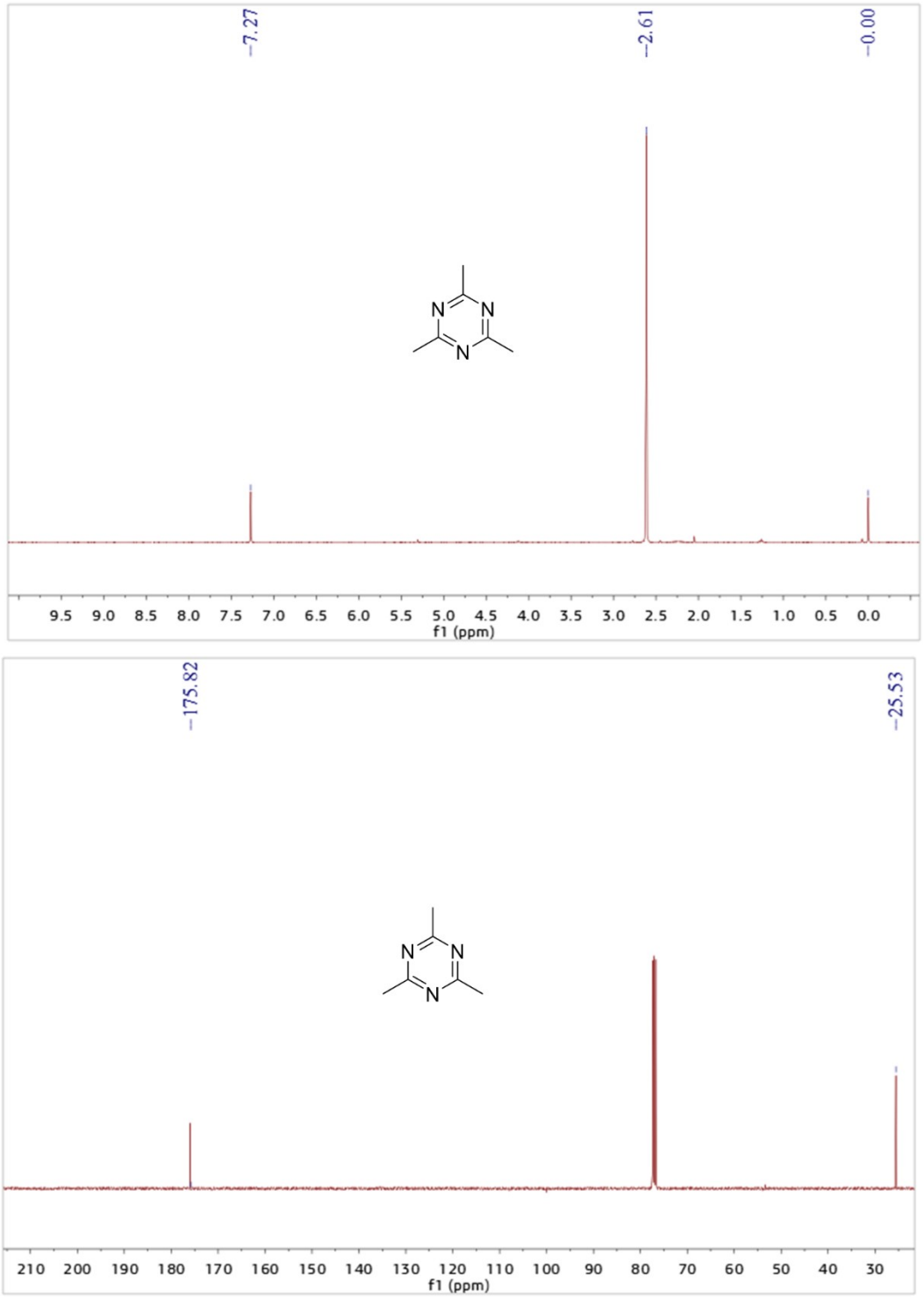

The ^{1}H-NMR and ^{13}C-NMR spectra of TMT

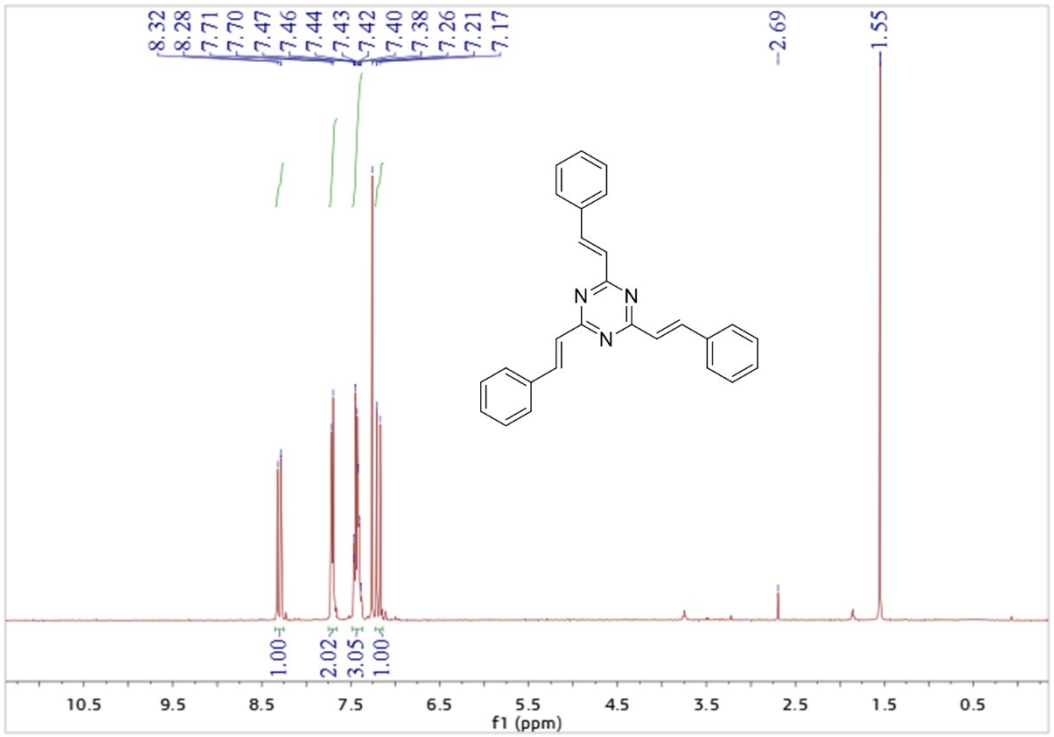

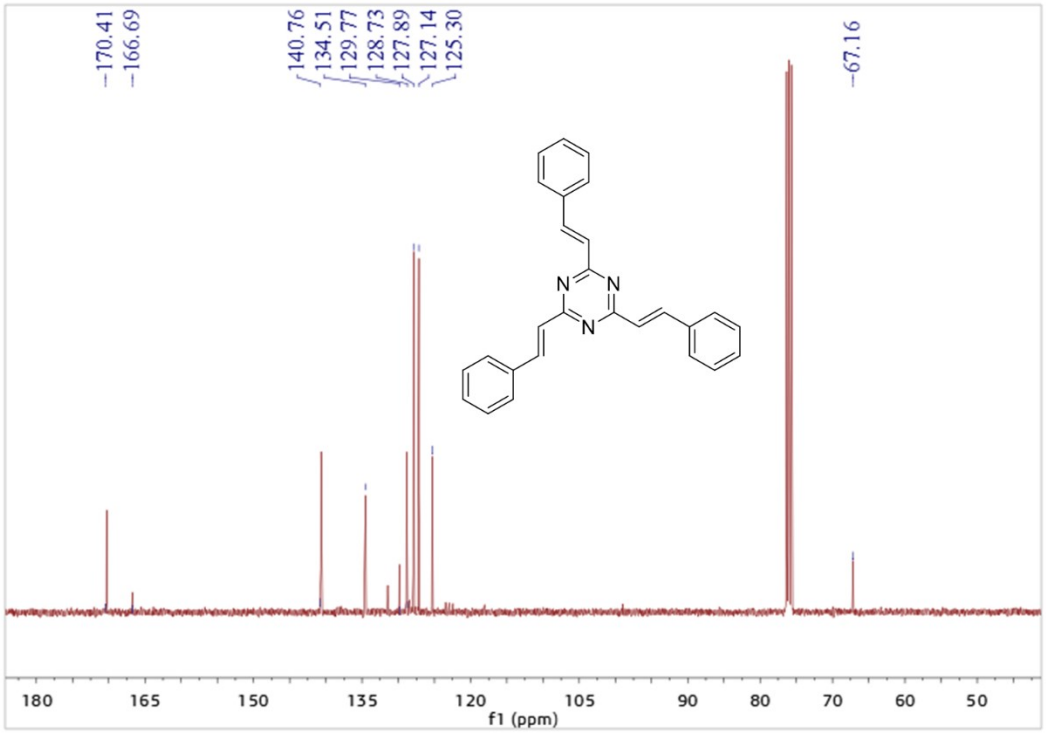

The [1]H-NMR and [13]C-NMR spectrum of TST

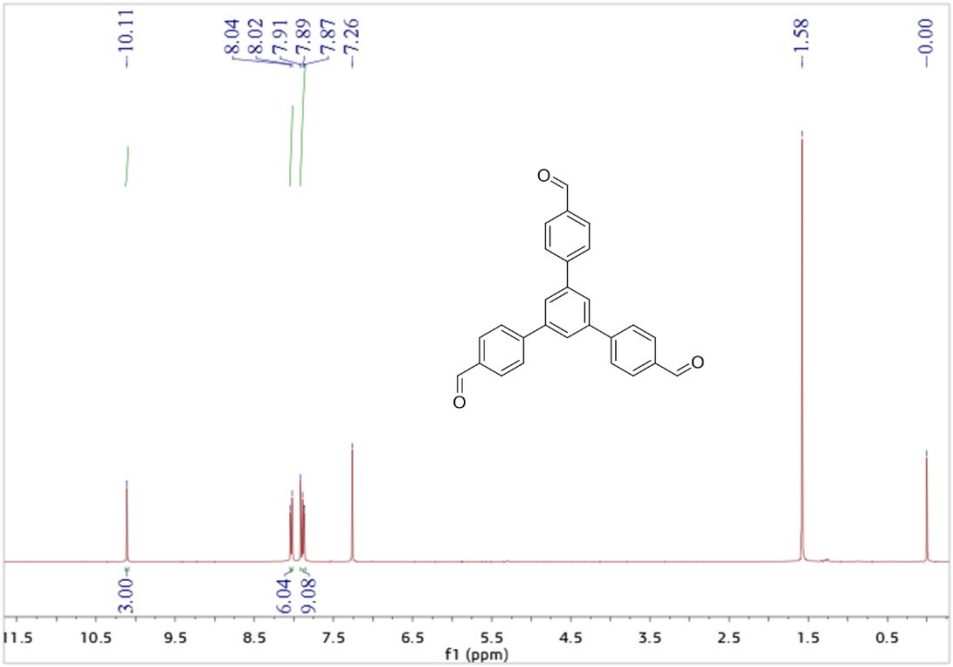

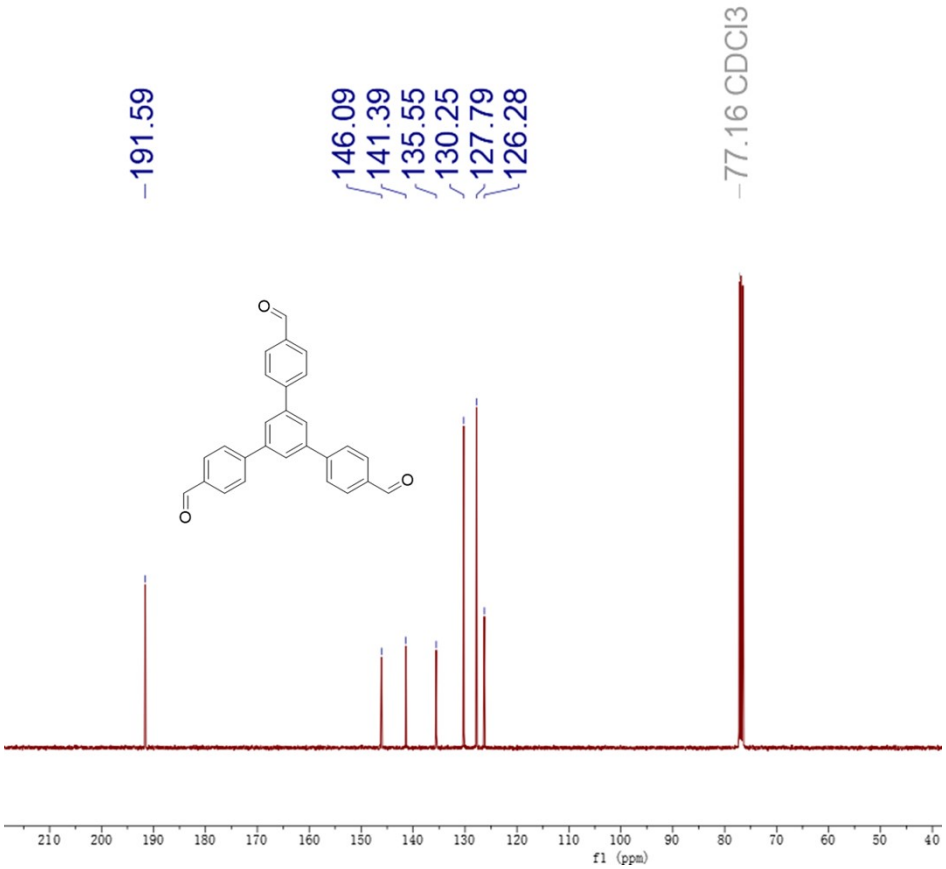

The ^{1}H-NMR and ^{13}C-NMR spectrum of TFPB

6. Reference

1 F. Xu, Z. Wang and Q. Gong, *Optical Materials*, 2007, **29**, 723–727.

2 J. Yang, A. Acharjya, M. Y. Ye, J. Rabeah, S. Li, Z. Kochovski, S. Youk, J. Roeser, J. Grüneberg, C. Penschke, M. Schwarze, T. Wang, Y. Lu, R. van de Krol, M. Oschatz, R. Schomäcker, P. Saalfrank and A. Thomas, *Angew Chem Int Ed*, 2021, **60**, 19797–19803.

3 G. Kresse and J. Furthmüller, *Phys. Rev. B*, 1996, **54**, 11169–11186.

4 J. P. Perdew, K. Burke and M. Ernzerhof, *Phys. Rev. Lett.*, 1996, **77**, 3865–3868.

5 G. Kresse and D. Joubert, *Phys. Rev. B*, 1999, **59**, 1758–1775.

6 X. Lian, J. Zhou, Y. You, Z. Tian, Y. Yi, J. Choi, M. H. Rümmeli and J. Sun, *Adv Funct Materials*, 2022, **32**, 2109969.

7 D. Zhang, P. Zhang, J. Yi, Q. Yuan, J. Jiang, Q. Xu, Z. Luo and X. Ren, *Journal of Alloys and Compounds*, 2011, **509**, 1206–1210.

8 L. Chen, L. Wang, Y. Wan, Y. Zhang, Z. Qi, X. Wu and H. Xu, *Adv. Mater,* 2020*,* **32***,* 1904433.

9 C. Krishnaraj, H. Sekhar Jena, L. Bourda, A. Laemont, P. Pachfule, J. Roeser, C. V. Chandran, S. Borgmans, S. M. J. Rogge, K. Leus, C. V. Stevens, J. A. Martens, V. Van Speybroeck, E. Breynaert, A. Thomas and P. Van Der Voort, *J. Am. Chem. Soc.*, 2020, **142**, 20107–20116.

10 W. Zhao, P. Yan, B. Li, M. Bahri, L. Liu, X. Zhou, R. Clowes, N. D. Browning, Y. Wu, J. W. Ward and A. I. Cooper, *J. Am. Chem. Soc.*, 2022, **144**, 9902–9909.

11 X. Zhang, J. Zhang, J. Miao, X. Wen, C. Chen, B. Zhou and M. Long, *Chemical Engineering Journal*, 2023, **466**, 143085.

12 W.-K. Han, H.-S. Lu, J.-X. Fu, X. Liu, X. Zhu, X. Yan, J. Zhang, Y. Jiang, H. Dong and Z.-G. Gu, *Chemical Engineering Journal*, 2022, **449**, 137802.

13 M. Kou, Y. Wang, Y. Xu, L. Ye, Y. Huang, B. Jia, H. Li, J. Ren, Y. Deng, J. Chen, Y. Zhou, K. Lei, L. Wang, W. Liu, H. Huang and T. Ma, *Angew Chem Int Ed*, 2022, **61**, e202200413.

14 Z. Zhou, M. Sun, Y. Zhu, P. Li, Y. Zhang, M. Wang and Y. Shen, *Applied Catalysis B: Environmental*, 2023, **334**, 122862.

15 M. Wu, Z. Shan, J. Wang, T. Liu and G. Zhang, *Chemical Engineering Journal*, 2023, **454**, 140121.

16 T. Yang, Y. Chen, Y. Wang, X. Peng and A. Kong, *ACS Appl. Mater. Interfaces*, 2023, **15**, 8066–8075.

17 J. Sun, H. Sekhar Jena, C. Krishnaraj, K. Singh Rawat, S. Abednatanzi, J. Chakraborty, A. Laemont, W. Liu, H. Chen, Y. Liu, K. Leus, H. Vrielinck, V. Van Speybroeck and P. Van Der Voort, *Angew Chem Int Ed*, 2023, **62**, e202216719.

18 L. Li, L. Xu, Z. Hu and J. C. Yu, *Adv Funct Materials*, 2021, **31**, 2106120.

19 G. Pan, X. Hou, Z. Liu, C. Yang, J. Long, G. Huang, J. Bi, Y. Yu and L. Li, *ACS Catal.*, 2022, **12**, 14911–14917.

20 H. Wang, C. Yang, F. Chen, G. Zheng and Q. Han, *Angew Chem Int Ed*, 2022, **61**, e202202328.

21 D. Chen, W. Chen, Y. Wu, L. Wang, X. Wu, H. Xu and L. Chen, *Angew Chem Int Ed*, 2023, **62**, e202217479.

22 L. Zhai, Z. Xie, C.-X. Cui, X. Yang, Q. Xu, X. Ke, M. Liu, L.-B. Qu, X. Chen and L. Mi, *Chem. Mater.*, 2022, **34**, 5232–5240.

23 Q. Zhi, W. Liu, R. Jiang, X. Zhan, Y. Jin, X. Chen, X. Yang, K. Wang, W. Cao, D. Qi and J.

Jiang, *J. Am. Chem. Soc.*, 2022, **144**, 21328–21336.
24 Y. Yang, J. Kang, Y. Li, J. Liang, J. Liang, L. Jiang, D. Chen, J. He, Y. Chen and J. Wang, *New J. Chem.*, 2022, **46**, 21605–21614.
25 F. Tan, Y Zheng, Z. Zhou, H. Wang, X. Dong, J. Yang, Z. Ou, H. Qi, W. Liu, Z. Zheng, X. Chen. *CCS Chem*. 2022, **4**, 3751–3761.
26 P. Das, G. Chakraborty, J. Roeser, S. Vogl, J. Rabeah and A. Thomas, *J. Am. Chem. Soc.*, 2023, **145**, 2975–2984.
27 X. Di, X. Lv, H. Wang, F. Chen, S. Wang, G. Zheng, B. Wang and Q. Han, *Chemical Engineering Journal*, 2023, **455**, 140124.
28 L. Li, L. Xu, Z. Hu and J. C. Yu, *Adv Funct Materials*, 2021, **31**, 2106120.
29 C. Wu, Z. Teng, C. Yang, F. Chen, H. B. Yang, L. Wang, H. Xu, B. Liu, G. Zheng and Q. Han, *Advanced Materials*, 2022, **34**, 2110266.
30 Y. Luo, B. Zhang, C. Liu, D. Xia, X. Ou, Y. Cai, Y. Zhou, J. Jiang and B. Han, *Angew Chem Int Ed*, 2023, **62**, e202305355.
31 Y. Liu, W.-K. Han, W. Chi, Y. Mao, Y. Jiang, X. Yan and Z.-G. Gu, *Applied Catalysis B: Environmental*, 2023, **331**, 122691.
32 T. Xu, Z. Wang, W. Zhang, S. An, L. Wei, S. Guo, Y. Huang, S. Jiang, M. Zhu, Y.-B. Zhang and W.-H. Zhu, *J. Am. Chem. Soc.*, 2024, jacs.4c04244.
33 M. G. Schwab, B. Fassbender, H. W. Spiess, A. Thomas, X. Feng and K. Müllen, *J. Am. Chem. Soc.*, 2009, **131**, 7216–7217.
34 J. Bi, W. Fang, L. Li, J. Wang, S. Liang, Y. He, M. Liu and L. Wu, *Macromol. Rapid Commun.*, 2015, **36**, 1799–1805.